

## ROLL-TO-ROLL PRINTED SOLAR CELLS: UP-SCALING FROM LABORATORY TO MEGAWATTS OF PRODUCTION

David Jackrel<sup>1</sup>, Ben Cardozo<sup>1</sup>, Francois Jacob<sup>1</sup>, Gregory Brown<sup>1</sup>, Peter Stone<sup>1</sup>, Jacob Woodruff<sup>1</sup>, Gregory Kimball<sup>1</sup>,  
Patrick Jeffries<sup>1</sup>, Wei Zhang<sup>1</sup>, Vladimir Faifer<sup>1</sup>, Jack Krawczyk<sup>1</sup>

<sup>1</sup>Nanosolar, Inc.  
San Jose, CA 95138 USA

**ABSTRACT:** Thin film photovoltaics (PV) offer the prospect of being significantly lower cost than traditional silicon panels at competitive efficiencies. Some of the most promising absorber materials being commercialized are CuInSe<sub>2</sub>-based (CIGS) due to demonstrated laboratory efficiencies over 20% [1, 2]. However, production module efficiencies are typically considerably lower than the best laboratory results. Nanosolar CIGS solar cells are produced using a low-cost non-vacuum printing method on flexible foil. This paper describes the practices that have been developed at Nanosolar to transfer laboratory processes to MW-scale manufacturing processes, at near-equivalent efficiencies. This has been accomplished by 1) developing laboratory equipment and processes that can predictably mimic manufacturing processes, 2) utilizing statistically valid experimental methods of optimization in the lab and manufacturing lines, and 3) establishing a deep fundamental understanding of the technology to aid in transferring concepts rather than rote recipes. We compare laboratory and manufacturing line efficiency distributions for different generations of Nanosolar cells and discuss the methodology which allows for efficient transfer of laboratory breakthroughs into mass production.

**Keywords:** CuInSe<sub>2</sub>, Nanoparticles, Solar Cell Efficiencies, Experimental Methods, Simulation

### 1 INTRODUCTION

Thin film photovoltaics (PV) have the potential to be significantly lower cost than traditional silicon panels at competitive efficiencies. The highest efficiency thin film PV devices are CuInSe<sub>2</sub>-based (CIGS), with demonstrated laboratory efficiencies over 20% [1, 2]. However, the efficiencies of panels in large-scale production are considerably lower than the best laboratory results.

Nanosolar has a coupon-based laboratory, and roll-to-roll pilot and manufacturing lines. The primary difference between the pilot line and the manufacturing line is that the throughput of the pilot tools is significantly lower than the throughput of the manufacturing tools. However, the pilot line produces devices that have the same form factor as those from the manufacturing line.

This paper describes the methodology that Nanosolar employs to transfer technologies from the laboratory to large scale manufacturing at nearly equivalent median efficiencies.

### 2 EXPERIMENTAL

CIGS devices in the laboratory were grown by a method similar to that described in [3]. Briefly, aluminum foil was used as a substrate. A thin barrier layer and Mo bottom contact were deposited followed by printing of a nanoparticle ink. The coated substrate went through atmospheric pressure rapid thermal processing to form a high quality CIGS layer followed by chemical bath deposition of CdS. This step was followed by deposition of a ZnO bi-layer. A Ni-Al grid pattern was deposited by e-beam evaporation and photolithography was used to define pixels, which are 0.5 cm<sup>2</sup>. For the 17.1% device, a MgF<sub>2</sub> anti-reflection (AR) coating was deposited by thermal evaporation. Devices were characterized by light current-voltage (I-V), external quantum efficiency (EQE), spectral photoluminescence (PL) and electron beam induced current (EBIC)

measurements.

CIGS devices in manufacturing share virtually the same device stack as those in the laboratory, however, manufacturing devices have a metal wrap through (MWT) architecture. A schematic and cross-section of the MWT architecture is shown in Figure 1. A via hole is created in the device stack and the cell foil, which conducts current from the fingers on the top electrode of the device stack through the via to the back foil. The cell foil and the back foil conduct the current laterally to the tabbed contacts of the cell. The cell foil tab of one cell and the back foil tab of an adjacent cell are connected to form a series circuit within a panel. Nanosolar MWT cells are roughly 220 cm<sup>2</sup> consisting of 220 vias, but have very low series resistance, since the current is conducted long distances through the foils, rather than thin deposited top and bottom contacts.

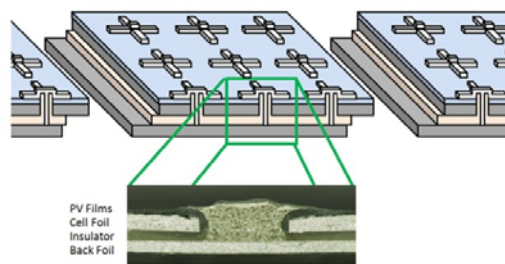


**Figure 1:** Nanosolar MWT architecture, illustrating how cells are connected within a panel, and a cross-section image of a single via.

### 3 RESULTS AND DISCUSSION

The first generation of Nanosolar cells produced median 11.9% total area efficiency small area cells (0.5 cm<sup>2</sup>) in the laboratory throughout 2009-2010 and an NREL certified champion cell at 15.3% (with anti-reflection coating). This first generation was successfully transferred to the manufacturing line and optimized

through several iterations of designed experiments to produce ~10 MW of large area cells (220 cm<sup>2</sup>). Laminated large area single cell test modules, randomly sampled from all production runs from this process produced a median efficiency of 11.5%, signaling a successful transfer of the laboratory process. These cells produced 10% efficient panels (2 m<sup>2</sup>) mainly due to module active area losses (for instance, from the edge seal). The second generation Nanosolar process produced median 12.7% total area efficiency cells in the laboratory, 12.5% laminated single-cell test modules on the manufacturing line, and 11-11.5% panels in production, again demonstrating the capability of the Nanosolar manufacturing process to nearly match laboratory, small-scale device efficiencies. The third generation of Nanosolar cells had a median total area efficiency of roughly 15% in the laboratory and an NREL certified champion cell at 17.1% (with anti-reflection coating). This third generation, which is currently being transferred to the manufacturing line, is projected to yield panels that are above 13% total area efficiency based on the results of the two previous generations. A comparison of the efficiency distributions for the first two generations in the laboratory and manufacturing line is shown in Figure 2.

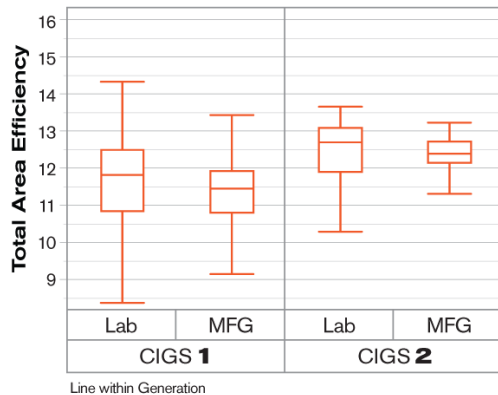


**Figure 2:** Total area efficiency distributions comparing lab small area cells and manufacturing single cell test modules for different generations of Nanosolar CIGS, showing quartiles and upper/lower fences.

The laboratory to manufacturing technology transfer was accomplished by 1) developing laboratory equipment and processes that can predictably mimic manufacturing processes, 2) utilizing statistically valid experimental methods of optimization in the lab and manufacturing lines, and 3) establishing a deep fundamental understanding of the technology to aid in transferring concepts rather than rote recipes.

### 3.1 Equipment and processes

The first component of our successful technology transfer is accomplished by developing laboratory equipment based on coupon substrates which can predictably mimic full scale roll-to-roll manufacturing processes. Such equipment aids development because of its low cost, fast construction and great flexibility, yet maintains similar underlying physical principals to the larger, high speed production tools. An example of this is shown in Figure 3, which compares the printing processes in the laboratory and manufacturing line. In

the laboratory, using a moving printing head over small, stationary coupons, in contrast to roll-to-roll coating in the manufacturing line, allows rapid testing of new ink formulations with low materials consumption.

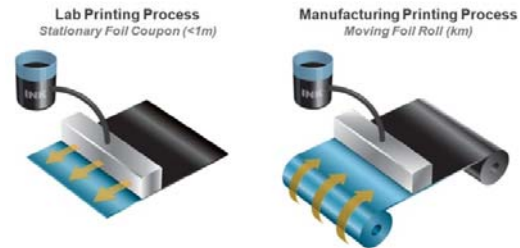


**Figure 3:** Schematic diagrams demonstrating the concepts of printing in the lab on stationary coupons with a moving print head (left) compared to roll-to-roll, which uses a stationary print head and moving web (right)

### 3.2 Statistically valid experimental methods

Another important component to transfer technology is to optimize processes utilizing statistically valid experimental methods such as designed experiments. Use of designed experiments in both the laboratory and manufacturing lines allows simultaneous study of multiple process parameters and their interactions in a statistically significant manner and with a minimum number of experimental runs. The generation 3 Nanosolar process was developed at laboratory scale by running a resolution V partial factorial experiment over six parameters known to affect absorber growth. Figure 4 (a) compares measured total area efficiency for laboratory devices to a linear model based on the experimental design. The red-dashed lines are 95% confidence intervals of the linear model fit. They do not overlap with the horizontal blue line which is a fit assuming all model terms of zero. Therefore, we can attribute the differences in efficiency from run-to-run in this experiment to statistically significant effects of changing parameter levels; if the spread in data was due to random noise we would expect the blue line to be contained in the confidence intervals. The effect of changing two parameters identified as significant on efficiency is shown in the contour plot in Figure 4 (b). A strong two factor interaction is visible in this contour plot. At the high level (+1) of X3 changing the level of X2 has little effect on efficiency. On the other hand at the low level (-1) of X3 changing the level of X2 affects efficiency by close to 1% absolute. The beneficial effect of low X3 is also visible as a main effect. This model led us to focus development of the third generation lab baseline process around the low levels of X2 and X3. The predicted total area efficiency of 15.1% from the experimental model agrees well with the measured distribution of large numbers of devices produced from the final baseline process (*c.f.* Figure 2).

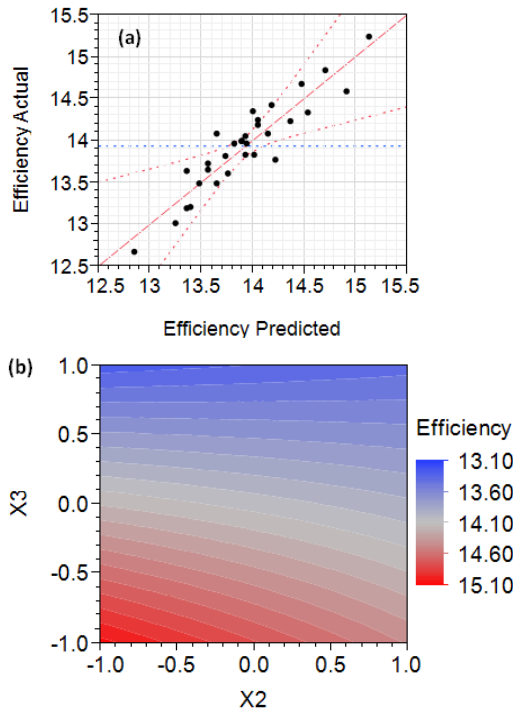


**Figure 4:** (a) Leverage plot of measured versus modeled efficiency from a 6 factor designed lab experiment on absorber growth conditions. (b) Contour plot of modeled efficiency in the reduced coordinate space of two significant factors from this experiment predicting 15% total area efficiency for a process combining the low levels (-1) of factors X2 and X3.

Due to differences between research equipment and the manufacturing line, technology transfer begins by the transfer of concepts rather than exact process conditions. We utilize designed experiments to identify important process parameters to focus on during manufacturing development. As an example, an experiment was run on the pilot line to examine the effect of four parameters known to affect absorber growth. Results of this experiment are summarized in the normal plot in Figure 5. Points falling on the normal line are likely due to random noise, while those which deviate from it are active effects. These results led us to focus on parameters X1 and X4 and to be wary of their mutual interaction when transferring the process to the manufacturing line. Additionally, this experiment alerted us to the possibility of a local optimum (negative quadratic term) within the parameter space. An equally important conclusion was that X2 and X3 had little effect on efficiency, which allowed us to deprioritize studying these parameters. Narrowing down the list of significant parameters at an early stage is essential to achieving efficient and rapid transfer of emerging technologies to full manufacturing capacity.

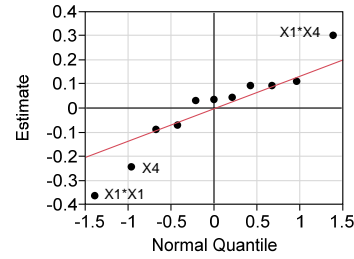


**Figure 5:** Normal quantile plot of model parameter estimates from a four-factor experiment. The red line is a normal line with slope equal to the standard error of the model. The parameter estimates are in units of total area efficiency.

### 3.3 Fundamental understanding

One of the most critical steps towards transferring technologies between the laboratory and manufacturing equipment is a fundamental understanding of efficiency improvements. The identification of materials signatures and ability to model the underlying mechanisms behind technologies developed in the laboratory provide valuable direction when introducing these technologies to the manufacturing line. Several characterization techniques are used to determine the materials signatures of each layer in the thin film stack, which are then used to transfer the technology into production. These material signatures can also be used in numerical simulations of the final device to determine the impact of each layer on the device efficiency.

The electrical characteristics of the final device are simulated using a combination of numerical models. Briefly, the 1-D I-V, external quantum efficiency (EQE) and spectral photoluminescence output of the thin film stack are simulated using a finite-element model to simultaneously solve Poisson's and the drift-diffusion equations for the device under illumination and electrical bias. This model incorporates all the necessary electrical and optical properties of each layer in the thin film stack and allows for bandgap grading within the CIGS absorber. Furthermore, in the cases where the device exhibits a distribution of electronic properties on the micro-scale, the model is run multiple times with a range of input parameters and the final I-V curve is then constructed using a simplified equivalent circuit model combining the results of the finite element simulations. Thin film optical interference effects are incorporated as a correction to the final device I-V curve based on a separate numerical model using the transfer-matrix method. Finally, to incorporate both macroscopic fluctuations in device properties and the MWT architecture, an equivalent circuit model of the device is built and solved using SPICE with each node in the circuit using the I-V output of the finite-element simulation. Put together, these simulations are able to connect the measured material properties of each individual layer with the final device characteristics (Jsc, Voc, FF, spectral response, etc).

One example of this is shown in Figure 6 where spectral photoluminescence (PL) is used to determine both the macro and microscopic bandgap distributions in the absorber. The emission spectrum is measured locally with a ~100 μm diameter laser and is fit following the approach of reference [4] where a Gaussian distribution of bandgaps is assumed to exist on a length scale smaller than the electronic diffusion length. An X-Y translational stage is then used to map the entire coupon providing accurate

information of the microscopic bandgap distributions over macroscopic areas.

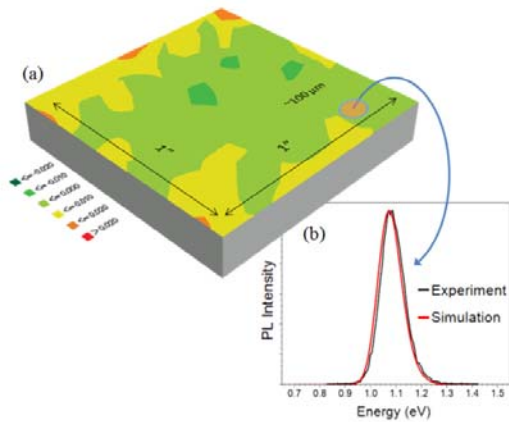


**Figure 6:** (a) 2-D map showing the macroscopic deviation in bandgap from the average bandgap over a 1x1 cm area (in eV). The bandgap is determined at each point by fitting spectral photoluminescence data obtained over a ~100 μm diameter spot as shown in (b).

The distribution of bandgaps within the absorber is just one of many properties of the device which govern its electrical behavior. An example of a specific type of device response that can be modeled from this and other materials information is the spectral response of the cell. An example EQE curve of a Nanosolar device is shown in Figure 7 along with the simulated quantum efficiency based on measurements of individual layers in the device stack. Of particular interest is the response of the device between the wavelengths of 0.8 and 1.2 μm as QE losses in this region can be driven by several sources and it's not generally obvious which mechanisms are driving this loss.

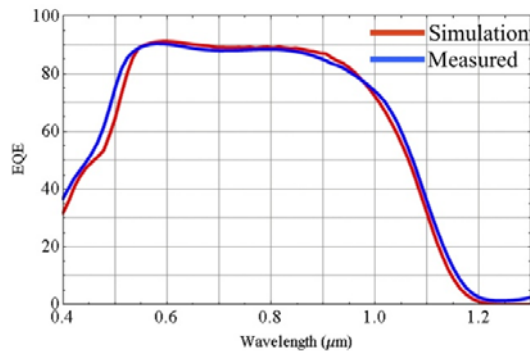


**Figure 7:** External quantum efficiency (EQE) of a Nanosolar device as measured and simulated. The simulated curve is obtained using a numerical model, which takes material parameter inputs determined by separate measurement techniques and simulates the expected cell response.

For this reason, additional characterization techniques are employed to determine the necessary parameters required to simulate the device EQE. These parameters include the aforementioned bandgap distributions laterally, the bandgap distribution within the depth of the film, minority carrier collection length (obtained from EBIC measurements [5]), and TCE free carrier

absorption among others. These opto-electronic parameters are determined using separate characterization techniques and then combined together in the numerical model described above. As apparent in Figure 7, the simulated curves provide a reasonable description of the actual spectral response of the device. It should be noted that this modeling approach can accurately fit a wide range of devices produced at Nanosolar while relying only on measured physical and electronic inputs and without modifying any free parameters in the model. This approach enables each individual source of current loss to be traced back to a particular property within a layer. With this information, it's then possible to focus laboratory efforts on potential areas of efficiency improvements, which can then be transferred to the production line.

In addition to the fundamental understanding of how each layer affects the properties of the final device, it's also critical to model the influences of cell architecture to maximize the efficiency of the final product. While the laboratory uses small area devices with evaporated fingers to quickly drive materials improvements, the production line uses an MWT structure, which is fundamentally different from the lab architecture. For this reason, equivalent circuit models are used to connect how changes in the electronic properties of the device will manifest themselves in the panel power output. An example of a simplified equivalent circuit model of a device is shown in Figure 8.

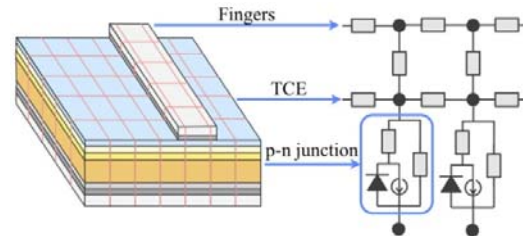


**Figure 8:** Simplified equivalent circuit diagram of a Nanosolar device. The effect of changing one layer of the cell can be simulated to determine the net impact on the overall device performance.

Using these equivalent circuit models, it is possible to determine the optimized device architecture based on the combined properties of the p-n junction, transparent conducting electrode (TCE) and finger/via pattern. Furthermore, as materials improvements are made which fundamentally change the accessible design space for each component of the final device (e.g. changes to the p-n junction, which increase the cell current), the numerical models enable efficient re-optimization of the entire structure. The ability to model the complex interactions of each layer on the final device performance reduces the need for empirical optimization of the cell architecture with every change to the process.

Finally, the equivalent circuit modeling shown in Figure 8 has also been extended beyond predicting standard test conditions (STC) and towards predicting the total energy production (TEP) by the panel over a certain time and location in the field. The primary difference between optimizing for STC versus TEP is the non-linear response of device efficiency with illumination conditions. Essentially, the cell responds linearly in short-circuit current with changes in illumination but non-linearly in fill factor and  $V_{oc}$ . As a result, the cell

architecture can be engineered to optimize performance for real-world conditions rather than STC. An example of this is given in Figure 9 where two different cell architectures are compared as a function of TCE sheet resistance in terms of STC and TEP. If optimizing for STC efficiency, the cell architecture is driven towards designs that minimize series resistance losses. Alternatively, in TEP calculations where the cell is often below 1-sun illumination, the optimal architecture shifts to reduce current losses (ex. free carrier absorption in the TCE) at the expense of higher series resistance. The net result is the cell architecture can be optimized using numerical modeling to maximize the energy produced in real world applications.

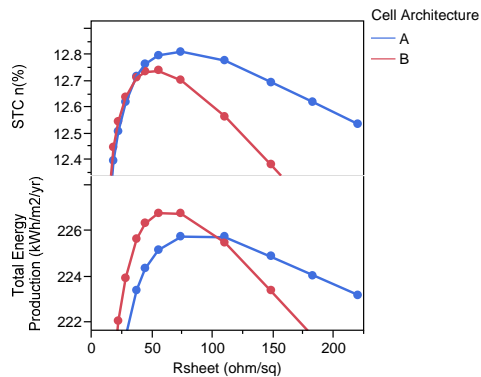


**Figure 9:** Simulated solar energy conversion efficiency of devices measured at standard test conditions (STC) and the estimated total energy production (TEP) over a year in Bakersfield, California. The preferred device architecture and TCE properties differ when optimizing for STC efficiency versus expected performance in the field.

#### 4 CONCLUSION

Two generations of Nanosolar technology have been transferred from the laboratory to volume manufacturing with similar median efficiencies; the first had roughly 11.5% median efficiency and the second roughly 12.5% median efficiency. The key methods driving laboratory to manufacturing technology transfer are by 1) developing laboratory equipment and processes that mimic manufacturing, 2) utilizing statistically valid experimental methods and 3) establishing a deep fundamental understanding of the technology. A third generation of Nanosolar technology has roughly 15% medians in the laboratory, which is projected to yield panels that are above 13% total area efficiency based on the results of the two previous generations.

#### 5 REFERENCES

- [1] P. Jackson et al., "New World Record Efficiency for Cu(In,Ga)Se<sub>2</sub> Thin-film Solar Cells Beyond 20%", *Prog. Photovoltaics* 19, 2011, pp. 894-897.
- [2] I. Repins et al., "19.9%-efficient ZnO/CdS/CuInGaSe<sub>2</sub> Solar Cell with 81.2% Fill Factor", *Prog. Photovoltaics* 16, 2008, pp. 235-239.
- [3] J. van Duren et al., "The Next Generation of Thin film Photovoltaics", *Thin-Film Compound*

*Semiconductor Photovoltaics*, MRS Symposia Proceedings No. 1012 (Materials Research Society, San Francisco, 2007), Y05.03.

- [4] J. Mattheis et al., "Light Absorption and Emission in Semiconductors with Band Gap Fluctuations - A Study on Cu(In,Ga)Se<sub>2</sub> thin films", *J. Appl. Phys.* **101**, 2007, 113519.
- [5] G. Brown et al., "Quantitative Imaging of Electronic Nonuniformities in Cu(In,Ga)Se<sub>2</sub> Solar Cells", *J. Appl. Phys.* **108**, 2010, 074516.